

# Isolation of Thioinosine and Butenolides from a Terrestrial *Actinomyces* sp. GSCW-51 and Their *in Silico* Studies for Potential against SARS-CoV-2

Mamona Nazir,<sup>\*a</sup> Muhammad Imran Tousif,<sup>\*b</sup> Muhammad Khalid,<sup>c</sup> Shehla Parveen,<sup>a</sup> Naseem Akhter,<sup>a</sup> Nosheen Farooq,<sup>a</sup> Muhammad Usman Khan,<sup>d</sup> Rana Farhat Mehmood,<sup>b</sup> Mohamad Fawzi Mahomoodally,<sup>e</sup> Shabbir Muhammad,<sup>f</sup> and Saleh S. Alarfajif

<sup>a</sup> Department of Chemistry, Government Sadiq College Women University, Bahawalpur, 63100, Pakistan, e-mail: mamonanazir.de@gmail.com

<sup>b</sup> Department of Chemistry, Division of Science and Technology, University of Education Lahore, Lahore, 32200, Pakistan, e-mail: Imran.tousif@ue.edu.pk

<sup>c</sup> Department of Chemistry, Khwaja Fareed University of Engineering & Information Technology, Rahim Yar Khan, 64200, Pakistan

<sup>d</sup> Department of Chemistry, University of Okara, Okara, 56300, Pakistan

<sup>e</sup> Department of Health Sciences, Faculty of Medicine and Health Sciences, University of Mauritius, 230 Réduit, Mauritius

<sup>f</sup> Department of Chemistry, College of Science, King Khalid University, P.O. Box 9004, Abha 61413, Saudi Arabia

In our continuous screening for bioactive microbial natural products, the culture extracts of a terrestrial *Actinomyces* sp. GSCW-51 yielded two new metabolites, *i.e.*, 5-hydroxymethyl-3-(1-hydroxy-6-methyl-7-oxooctyl)dihydrofuran-2(3*H*)-one (**1**), 5-hydroxymethyl-3-(1,7-dihydroxy-6-methyloctyl)dihydrofuran-2(3*H*)-one (**2**), and two known compounds; 5'-methylthioinosine (**3**), and 5'-methylthioinosine sulfoxide (**4**), which are isolated first time from any natural source, along with four known compounds (**5–8**). The structures of the new compounds were deduced by HR-ESI-MS, 1D and 2D NMR data, and in comparison with related compounds from the literature. Additionally, owing to the current COVID-19 pandemic situation, we also computationally explored the therapeutic potential of our isolated compounds against SARS-CoV-2. Compound **4** showed the best binding energies of  $-6.2$  and  $-6.6$  kcal/mol for M<sup>pro</sup> and spike proteins, respectively. The intermolecular interactions were also studied using 2-D and 3-D imagery, which also supported the binding energies as well as put several insights under the spotlight. Furthermore, Lipinski's rule of 5 was used to predict the drug likeness of compounds **1–4**, which indicated all compounds obey Lipinski's rule of 5. The study of bioavailability radars of the compounds **1–4** also confirmed their drug likeness properties where all the five crucial drug likeness parameters are in color area, which is safe to be used as drugs. Our isolation and computational findings highly encourage the scientific community to do further *in vitro* and *in vivo* studies of compounds **1–4**.

**Keywords:** Terrestrial *Actinomyces*, thioinosine, butenolides, structure elucidation, *in silico* study, COVID-19.

## Introduction

The increasing resistance of microbes to antibiotics has become a major global issue. Infections caused by

multidrug resistant organisms, such as bacteria, fungi, and viruses, require therapeutics with novel chemical scaffolds and/or modes of action. The discovery of new natural compounds is still crucial for the development of new antimicrobial agents. The majority of antimicrobial medicines currently in use are of natural origin.<sup>[1]</sup> Actinobacteria remain a significant source of

Supporting information for this article is available on the WWW under <https://doi.org/10.1002/cbdv.202100843>

new secondary metabolites for drug development among natural sources of bioactive compounds. The most common group of microorganisms that produces the bioactive compounds is actinobacteria. They produce two-thirds of all naturally derived antibiotics used in medicine, veterinary medicine, and agriculture today. The majority of these compounds are from the genus *Streptomyces*.<sup>[1–3]</sup> Varied microorganisms isolated from different environments produced variety of novel bioactive compounds, particularly those who have unique chemical structures and biological importance.<sup>[4]</sup> *Actinomycetes*, the soil Gram-positive bacteria, are producing wide variety of bioactive secondary metabolites. More than 140 *Actinomycete* genera have been discovered so far, however, only few of these are studied for their bioactive chemicals.<sup>[5]</sup> Most common antibiotics provided by this group include tetracyclines, streptomycin, dactinomycin and streptothricin, erythromycin and its derivatives, chloramphenicol and rifamycins etc.<sup>[6]</sup> Ahmpatinin<sup>1</sup>Bu, pentapeptide 4862F are recognized as the strongest antiviral agents from *Actinomycetes*<sup>[1]</sup> besides, antimycin A1a is also a potent antiviral compound from *Actinomycetes*.<sup>[7]</sup> In the present study, a terrestrial *Actinomycete* sp. GSCW-51 was investigated for its bioactive secondary metabolites. Two new butenolides (**1** and **2**), two new natural thioinosine derivatives **3** and **4** (Figure 1) along with known compounds 3-methoxy-4,5-dihydroxybenzoic acid (**5**)<sup>[8]</sup> 3-methoxy-4-hydroxybenzoic acid (**6**),<sup>[9]</sup> tyrosol (**7**),<sup>[10]</sup> 4-(4'-hydroxyphenyl)butan-2-one (**8**)<sup>[11]</sup> were separated from the culture broth of this microorgan-

ism. Further, in recent global pandemic of COVID-19 caused by SARS-CoV-2 is proving destructive to the world communities without boundaries. There is dire need to check every possibility to find a much-needed therapeutic drug candidate for SARS-CoV-2. As describe above the compounds isolated from *Actinomycetes* have antiviral properties and due to recent scenario of covid-19 pandemic, the isolated metabolites from the *Actinomycetes* GSCW-51 were studies in *silico* against SARS-CoV-2. Along the above stated lines, the activity of selected *Actinomycetes* was also checked against the main protease M<sup>Pro</sup> and spike proteins of SARS-CoV-2 by using the molecular docking techniques. The M<sup>Pro</sup> and spike proteins play crucial roles in protein replication and attachment of virus to the host cells, respectively. So, the study of intermolecular interactions of *Actinomycetes* with these two crucial proteins can bring several novel insights the therapeutic effects of our isolated *Actinomycetes*. The aim and objectives of the current investigation are twofold; isolation and characterization of metabolites from the *Actinomycetes* GSCW-51 and to perform molecular docking analysis for studying antiviral potential against SARS-CoV-2 which has caused deadly pandemic of COVID-19.

## Results and Discussion

A 15 L shaker culture of the *Actinomycetes* GSCW-51 was extracted with ethyl acetate, and was subjected to repeated normal phase and reversed phase silica gel

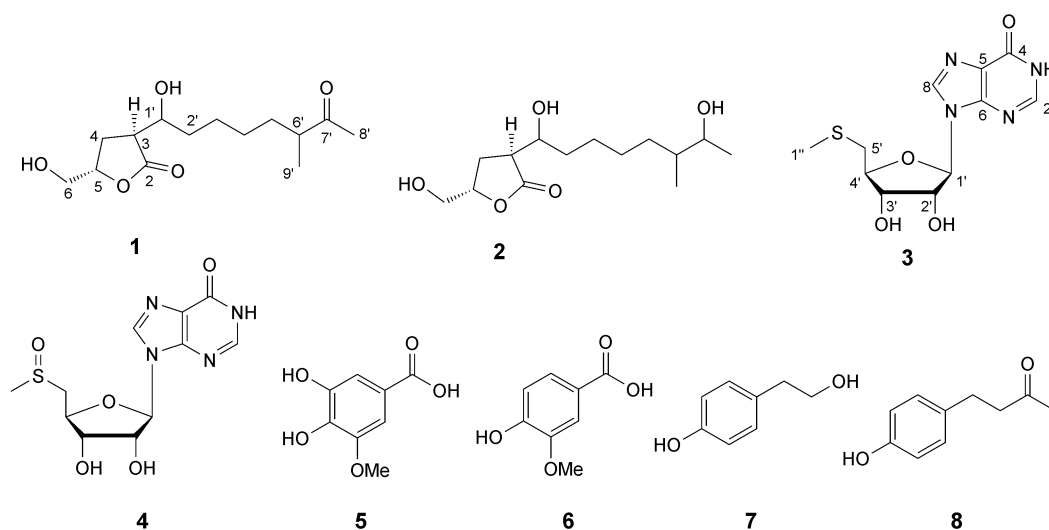


**Figure 1.** Structures of the compounds **1–8** isolated from culture broth of *Actinomycetes* GSCW-51.

column chromatography to get four new (**1–4**) and four known (**5–8**) compounds. All the isolates were characterized with the combination of several spectroscopic data. The ESI-MS in positive mode of **1** showed *pseudo*-molecular ion at  $m/z$  290  $[M + NH_4]^+$ , 562  $[2M + NH_4]^+$  and 295  $[M + Na]^+$  and 567  $[2M + Na]^+$ , whereas HR-ESI-MS analysis of the latter two ions at  $m/z$  295.1516  $[M + Na]^+$  and 567.3140  $[2M + Na]^+$  led to the molecular formula as  $C_{14}H_{24}O_5$  with 03 double bond equivalents (DBE). In the  $^1H$ -NMR spectrum of **1**, an acetyl methyl protons displayed their position at  $\delta$  2.10 (s,  $CH_3$ ), whereas a secondary methyl resonance at  $\delta$  1.07 (d,  $J=7.0$ , H-C(9'), 3H) was correlated in COSY spectrum (Figure 2) with a methine at  $\delta$  2.58–2.61 (m, 1H), which in turn interacted in COSY spectrum with a multiplet of various methylene groups at  $\delta$  1.42–1.62 (m, 6H) disclosed an aliphatic chain **1** ending with

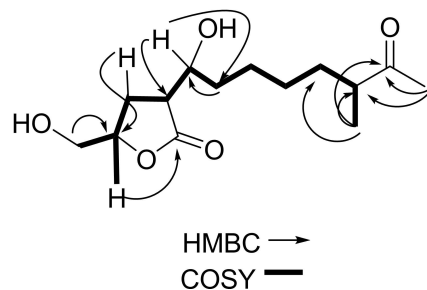


**Figure 2.** COSY and HMBC correlations observed in the spectra of **1**.

acetyl group. An oxymethine resonating at  $\delta$  4.01 (m, H-1') was also correlated with aliphatic methylene groups at  $\delta$  1.42–1.62 (m, 6H) and another methine at  $\delta$  2.79–2.81 (m, 1H), which in turn showed its further COSY correlation with aliphatic methylene proton signals at  $\delta$  2.38–2.40 (m, 2H) and 2.09–2.15 (m, 2H). The most downfield oxymethine at  $\delta$  4.57–4.60 (m, 1H) could be correlated in COSY spectrum with H-4a and H-4b and with an oxygenated methylene at 3.74 (dd,  $J=12.3$ , 3.1, H-C(6a), 1H) and 3.59 (dd,  $J=12.3$ , 4.1, H-C(6b), 1H). Careful analysis of the COSY spectrum (Figure 2) of **1** established an 11-carbon chain (C-6-C-9'), which were substantiated through  $^{13}C$ -NMR spectral analysis (Table 1).

Other three carbon nuclei displayed their positions in  $^{13}C$ -NMR spectrum at  $\delta$  179.9 (C-2), 214.4 (C-7') and 26.6 (C-8').  $\gamma$ -Lactone formation in **1** could be established due to HMBC (Figure 2) of H-5 ( $\delta$  4.57–4.60) with carbonyl carbon at  $\delta$  179.9 (C-2). Further, H-4 ( $\delta$  2.38–2.40 and 2.09–2.15), H-3 ( $\delta$  2.79–2.81) and H-1' ( $\delta$  4.01–4.09) also showed HMBC with lactone carbonyl (C-2). Secondary methyl protons (H-9') were found interacting with ketonic carbon ( $\delta$  214.4, C-7'), aliphatic methine at  $\delta$  46.7 (C-6') and methylene carbon at  $\delta$  26.8 (C-5'). Other HMBCs (Figure 2) and combination of HSQC data finally offered the structure of **1** as a new butanolide 5-hydroxymethyl-3-(1-hydroxy-6-methyl-7-oxooctyl)dihydrofuran-2(3H)-one. The relative configuration in the lactone ring was

**Table 1.** NMR data of **1** and **2** ( $CD_3OD$ , 600, 125 MHz).

Position	<b>1</b>			<b>2</b>	
	$^1H$ , $\delta$	COSY, $\delta$	$^{13}C$ , $\delta$	$^1H$ , $\delta$	COSY, $\delta$
2	–	–	179.9 (C)	–	–
3	2.79–2.81, (m)	4.01–4.09, 2.38–2.40, 2.09–2.15	46.1 (CH)	2.78–2.81 (m)	2.30–2.41, 2.09–2.19, 4.03–4.19
4	2.38–2.40, 2.09–2.15 (m)	2.79–2.81, 4.57–4.60	22.8 ( $CH_2$ )	2.30–2.41, 2.09–2.19 (each m)	2.78–2.81, 4.58–4.63
5	4.57–4.60 (m)	2.38–2.40, 3.74, 3.59	79.8 (CH)	4.58–4.63 (m)	2.30–2.41, 2.09–2.19, 3.77
6	3.74 (dd, $J=12.3$ , 3.1), (3.59, dd, $J=12.3$ , 4.1)	4.57–4.60	63.6 ( $CH_2$ )	3.77 (dd, $J=12.4$ , 3.2), (3.57, m, $J=12.4$ , 4.3)	4.58–4.63
1'	4.01–4.09 (m)	2.38–2.40, 2.09–2.16, 1.67–1.69, 1.32–1.33	69.5 (CH)	4.03–4.19 (m)	2.78–2.81, 1.80–1.81
2'	1.67–1.69 (m), 1.32–1.33 (m)	4.01–4.09	32.5 ( $CH_2$ )	1.80–1.81 (m)	4.03–4.19
3', 4', 5'	1.42–1.62 (m)		25.6 (C-5', $CH_2$ ), 35.0 (C-3', $CH_2$ ), 26.8 (C-4', $CH_2$ )	1.38–1.42 (m)	
6'	2.58–2.61 (m)	1.07	46.7 (CH)	1.38–1.51 (m)	0.87
7'	–	–	214.4	3.59–3.64 (m)	1.23
8'	2.10 (s)	–	26.7 ( $CH_3$ )	1.23, 2 signals for doublet methyl	3.64
9'	1.07 (d, $J=7.0$ )	2.58–2.61	15.2 ( $CH_3$ )	0.87, 2 signals for doublet methyl, $J=6.9$	1.38

established based on NOESY experiments as 3*S*,5*R* (Figure 3); unfortunately, there was no coupling visible between 1'-H and 4'-H<sub>2</sub>. Compound **1** is a new member of a sub-class of butenolides with a 5-hydroxymethyl substituent. Nearly all butenolides known from microorganisms constitute a 1-hydroxyalkyl side chain at C-3, or are the corresponding  $\alpha,\beta$ -unsaturated ketones with exocyclic double bonds.<sup>[12]</sup> Their common examples are the tornabeatins,<sup>[13]</sup> however, the first compound of this type, (1'*R*,2*S*,4*S*)-2-(1-hydroxy-6-methylheptyl)-4-hydroxymethylbutanolide was reported from marine *Actinomyces*.<sup>[14,15]</sup> Also from plants only fewer butenolides have been published<sup>[16–18]</sup> or the saccopetrins.<sup>[19]</sup> Thus, the configuration at C-3 to C-5 and C-1' could be proposed due to comparable NMR values of these centers.

The HR-ESI-MS in positive mode of **2** revealed *pseudo*-molecular ion at  $m/z$  297.1675 [M+Na]<sup>+</sup> corresponding to the molecular formula of **2** as C<sub>14</sub>H<sub>26</sub>O<sub>5</sub> with same number of carbon and oxygen atoms but with one DBE lesser than that of **1**, which indicated **2** could be a reduced form of **1**. The <sup>1</sup>H-NMR spectrum was very similar to that of **1**, however, instead of the acetyl singlet, a methyl doublet was found at  $\delta$  1.23 (H-8'), which showed a COSY correlation with an oxygenated methine at  $\delta$  3.59–3.64 (m, 1H). As this compound had two double bond equivalents, it was obviously the corresponding alcohol **2**, obtained by reduction of 7'-C=O in **1**. The appearance the H-8' and H-9'-methyl doublets each into two overlapping signals is a hint for a mixture of diastereoisomers.<sup>[20]</sup> Low amount and limited lab facilities did not allow us to separate the diastereomeric mixture and thus planar structure was substantiated as **2**.

*Pseudo*-molecular ion peak in (+)-HR-ESI-MS at  $m/z$  299.08086 [M+H]<sup>+</sup>, 321.0628 [M+Na]<sup>+</sup> established the molecular formula of **3** as C<sub>11</sub>H<sub>14</sub>N<sub>4</sub>O<sub>4</sub>S. The <sup>1</sup>H-NMR spectrum displayed signals of six methine groups at  $\delta$  8.08 (s, H-C(2), 1H), 8.22 (s, H-C(8), 1H), 6.01 (d,  $J=5.0$ , H-C(1'), 1H), 4.71 (t,  $J=5.1$ , H-C(2'), 1H), 4.30 (t,  $J=5.0$ , H-C(3'), 1H), 4.21 (q,  $J=5.8$ , H-C(4'), 1H) one methylene at  $\delta$  2.92 (dd,  $J=14.1$ , 5.6, H<sub>a</sub>-C(5'),

1H), 2.88 (dd,  $J=14.1$ , 5.9, H<sub>b</sub>-C(5'), 1H) and a methyl group at  $\delta$  2.10 (s, H-C(1''), CH<sub>3</sub>). Consecutive COSY interactions from H-1' to H-5' disclosed a furanoside moiety in **3**, which could further be substantiated through <sup>13</sup>C-NMR spectrum (Table 2). Downfield carbon resonances at  $\delta$  158.9, 150.0, 146.8, 140.8 and 125.8 were in agreement with chemical shifts of hypoxanthine in osterine A<sup>[21]</sup> and the shimofuridins,<sup>[22]</sup> however, difference was found in C-chemical shifts of furanoside moiety where the up-field shift ( $\delta$  37.6) of the methylene signal pointed to a connection with sulfur instead of nitrogen or oxygen, respectively. The methylene protons showed HMBCs (Figure 4) with the methyl carbon resonance at  $\delta$  16.5 and vice versa indicating that sulfur is present between these groups; further HMBCs are shown in Figure 4.

These data and assignments made on the basis of HSQC finally disclosed compound **3** as 5'-methyl-5'-thioinosine, which is new as natural product, however, was synthesized previously,<sup>[23]</sup> the reported <sup>1</sup>H-NMR data were identical with our data within narrow limits. In biosynthetic pathway, compound **3** is proposed, as deaminated version of 5-methylthioadenosine, a known metabolite in the methionine salvage pathway. The structural variety of naturally occurring thiomethylpentosides is very low however, the closely related 5'-S-methyl-5'-thioadenosine has been isolated from various sources.<sup>[24]</sup>

Compound **4** was found to be sulfoxide analog of **3**, since the HR-ESI-MS in positive mode displayed *pseudo*-molecular ion peak at  $m/z$  315.07577 [M+H]<sup>+</sup> (calc. for C<sub>11</sub>H<sub>14</sub>N<sub>4</sub>O<sub>4</sub>S), 337.05771 [M+Na]<sup>+</sup> (calc. for C<sub>11</sub>H<sub>14</sub>N<sub>4</sub>O<sub>5</sub>S), thus leading to the formula C<sub>11</sub>H<sub>14</sub>N<sub>4</sub>O<sub>5</sub>S, with one oxygen atom more than in **3**. The <sup>1</sup>H and <sup>13</sup>C-NMR spectra (Table 2) were nearly identical to those of **3**, with exception of the downfield shifted signals for the C-5'-methylene and the S-methyl group, and a surprising doubling of most <sup>1</sup>H and <sup>13</sup>C-NMR signals (Table 2). Compound **4** is there-

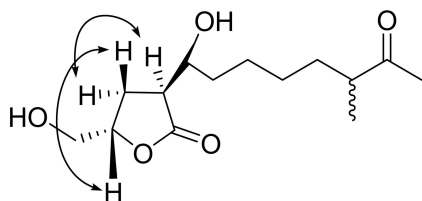


**Figure 3.** NOESY correlations observed in the spectrum of **1**.

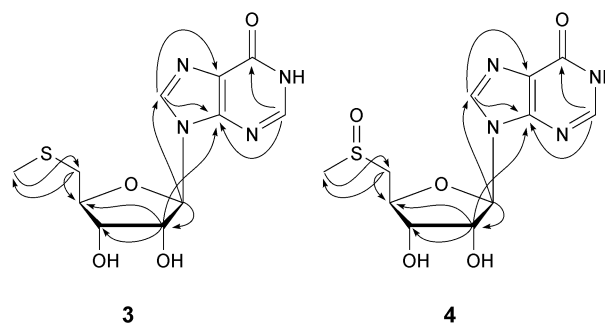


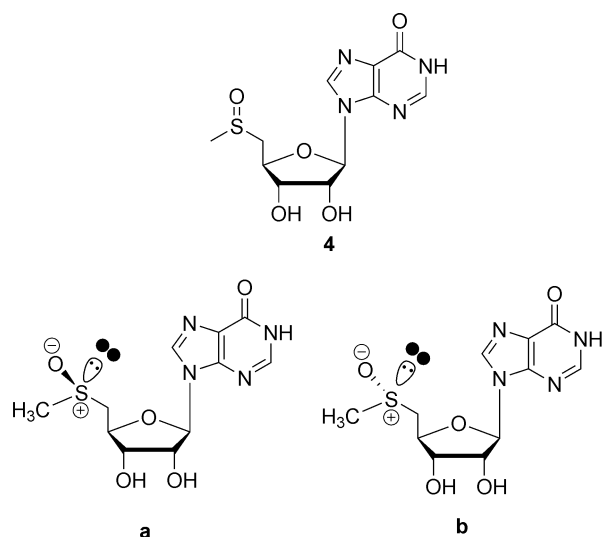
**Figure 4.** Identical HMBCs were observed in **3** and **4**.

**Table 2.**  $^1\text{H}$  and  $^{13}\text{C}$ -NMR data of **3** and **4** ( $\text{CD}_3\text{OD}$ , 600 and 125 MHz, respectively).

Position	<b>3</b>		<b>4*</b>	
	$^1\text{H}$ , $\delta$	$^{13}\text{C}$ , $\delta$	$^1\text{H}$ , $\delta$	$^{13}\text{C}$ , $\delta$
2	8.08, (s)	146.8 (CH)	8.02 (s)	146.87 146.85 (CH)
3	–	–	–	–
4	–	158.9 (C)	–	158.9 (C)
5	–	125.8 (C)	–	126.28 126.20 (C)
6	–	150.0 (C)	–	149.71 149.70 (C)
7	–	–	–	–
8	8.22 (s)	140.8 (CH)	8.20, 8.19 (1H each, s)	141.39 141.27 (CH)
1'	6.01 (d, $J=5.0$ )	90.2 (CH)	6.02 (d, $J=5.0$ )	91.25 91.24 (CH)
2'	4.71 (t, $J=5.1$ )	75.2 (CH)	4.80, 4.78 (1H each, t, $J=5.1$ )	74.81 74.74 (CH)
3'	4.30 (t, $J=5.0$ )	73.9 (CH)	4.51–4.53 (2H, m)	74.93 (2CH)
4'	4.21 (q, $J=5.8$ )	85.6 (CH)	4.23–4.36 (2H, m)	79.63 79.61 (CH)
5'	2.92 (dd, $J=14.1, 5.6$ ) 2.88 (dd, $J=14.1, 5.9$ )	37.4 ( $\text{CH}_2$ )	3.40 (dd, $J=14.2, 5.6$ ) 3.20 (dd, $J=14.2, 5.8$ ) 3.26 (m)	58.8 56.1 ( $\text{CH}_2$ )
1''	2.10 (s)	16.5 ( $\text{CH}_3$ )	2.68 (s)	38.1 38.5 ( $\text{CH}_3$ )

\*Values in duplicate due to diastereoisomers.

fore 5'-methylthioinosine sulfoxide and occurs as a mixture of diastereoisomers due to the chiral sulfenyl group (Figure 5).

**Figure 5.** Two diastereoisomeric forms of 5'-methylthioinosine sulfoxide (**4**).

It is an unusual metabolite, which was thought to be an artifact during isolation procedure, however, the possibility of such a non-specific oxidation is ruled out because of the use of non-oxidative isolation protocol. Further several sulfoxides are reported as natural products,<sup>[25]</sup> especially from *Allium* species.<sup>[26]</sup> In addition, *Streptomyces* (a genus of *Actinomycetes*) are used for enantioselective sulfoxidation of sulfides,<sup>[27]</sup> which authenticate compound **4** as a new natural product. As for **3**, the adenine derivative corresponding to **4** was described previously,<sup>[25]</sup> it is an inhibitor of platelet aggregation. Both **3** and **4** were inactive in cellular HIV tests. Due to the isolation of lesser amount we were not able to perform biological activities of these compounds, but the butenolides have gained special attention as  $\alpha$ -glucosidase, cytotoxic and anti-inflammatory agents.<sup>[28–30]</sup> Previous research has identified them as distinguishing characteristics of  $\alpha$ -glucosidase inhibitory actions. Recently butenolides showed the promising activity against the influenza viruses. A number of compounds were tested *in vitro* and *in vivo* against the influenza A virus H1N1 and was found that influenza A virus H1N1 could be inhibited by butenolides, by targeting the Neuraminidase

enzyme.<sup>[31]</sup> Further a natural butenolide (4*R*,6*S*)-2-dihydromenisdaurilide (DHMD), as an efficient inhibitor of Hepatitis C virus (HCV).<sup>[32]</sup> On the other hands, sulfur-containing purine nucleoside analogs were considering important agents, which inhibit the RNA viruses. Further sofosbuvir thio-analogs and 2'-deoxy-4'-thioribo purine nucleosides derivatives also showed good antiviral activity.<sup>[33–35]</sup> So, computationally study was also performed to explore the therapeutic potential of our isolated compounds against SARS-CoV-2 due to COVID-19 pandemic situation.

### Computational Study

#### Binding Energy and Inhibition Constants of Compounds 1–4 against SARS-CoV-2

The two most crucial parameters in molecular docking are binding interaction energy and inhibition constants for ligands docked with a macromolecule of target protein. The binding energies and inhibition constants have an inverse relationship where larger negative value of binding energy and lower value of inhibition constant indicates a good interaction between ligand and protein molecules.<sup>[36]</sup> The binding energies and inhibition constants for compounds 1–4 with M<sup>PRO</sup> and spike proteins were shown in Table 3. A careful analysis of Table 3 reveals that binding energy of compounds 1–4 with M<sup>PRO</sup> ranged from –5.1 to –6.2 kcal/mol and the increasing order (where negative sign indicates favorable interactions) of binding energies is 4 > 2 > 3 > 1 for M<sup>PRO</sup> protein. A graphical comparison among the binding energies of the all compounds for M<sup>PRO</sup> is shown in Figure 6 where the lowest and the most favorable energy is seen for compound 4 which is –6.2 kcal/mol. The binding energy of compounds 1–4 with spike protein ranged from –5.8 to –6.6 kcal/mol and their increasing order (where negative sign indicates favorable interactions)

of binding energies is 4 > 3 > 2 > 1 for spike protein. For more comprehensive understanding, a graphical comparison among the binding energies of the all compounds for spike protein is also shown in Figure 6 where the lowest and most favorable energy is also seen for compound 4. Among all compounds, compound 4 show the highest binding tendency to M<sup>PRO</sup> and spike proteins with its binding energies which are –6.2 and –6.6 kcal/mol, respectively. The inhibition constants of the best dock compound 4 are found to be 24.46 and 13.94 μmol for M<sup>PRO</sup>, and spike proteins, respectively. These results showed that among all the compounds, compound 4 exhibits reasonably good binding energies for both proteins of SARS-CoV-2, which are docked to the catalytic sites of M<sup>PRO</sup> and spike proteins. Additionally, we have performed docking studies for two positive control compounds including Remdesivir and Nirmatrelvir which are well-known COVID-19 drug compounds.<sup>[37]</sup> Nirmatrelvir is very recently approved oral drug as developed by Pfizer, which also an M<sup>PRO</sup> enzyme inhibitor.<sup>[38]</sup> For comparative purpose, we have performed docking of Remdesivir and Nirmatrelvir under the similar calculation conditions. The binding energy for M<sup>PRO</sup> enzyme with Remdesivir and Nirmatrelvir are found to be –5.7 and –6.4 kcal/mol while for spike protein with Remdesivir and Nirmatrelvir these are found to be –7.6 and –6.5 kcal/mol (see Table 3). A semi-quantitative comparative analysis indicates that our compound 4 possesses comparable binding energies to Remdesivir and Nirmatrelvir drug compounds. A detail docking analysis including 3-D and 2-D diagrams of Remdesivir and Nirmatrelvir complexed with both M<sup>PRO</sup> and spike proteins were given in Figure S1 of Supporting Information of the article. Furthermore, it will be also interesting to compare the calculated binding energies of above entitled compounds with those of other similar studies. For instance, thiazole-based heterocyclic

**Table 3.** Binding energy (kcal/mol) and inhibition constant (Kd) of docked compounds (1–4) and known drugs with M<sup>PRO</sup> and spike proteins.

Ligands	Targeted Protein	Binding Energy (kcal/mol)	Inhibition Constant (μmol)	Ligands	Targeted Protein	Binding Energy (kcal/mol)	Inhibition Constant (μmol)
1	M <sup>PRO</sup>	–5.3	126.16	1	Spike	–5.8	54.08
2		–5.7	64.07	2		–5.9	45.69
3		–5.4	106.51	3		–6.2	27.48
4		–6.2	27.46	4		–6.6	13.99
Remdesivir		–5.7	64.07	Remdesivir		–7.6	2.56
Nirmatrelvir		–6.4	19.57	Nirmatrelvir		–6.5	16.52

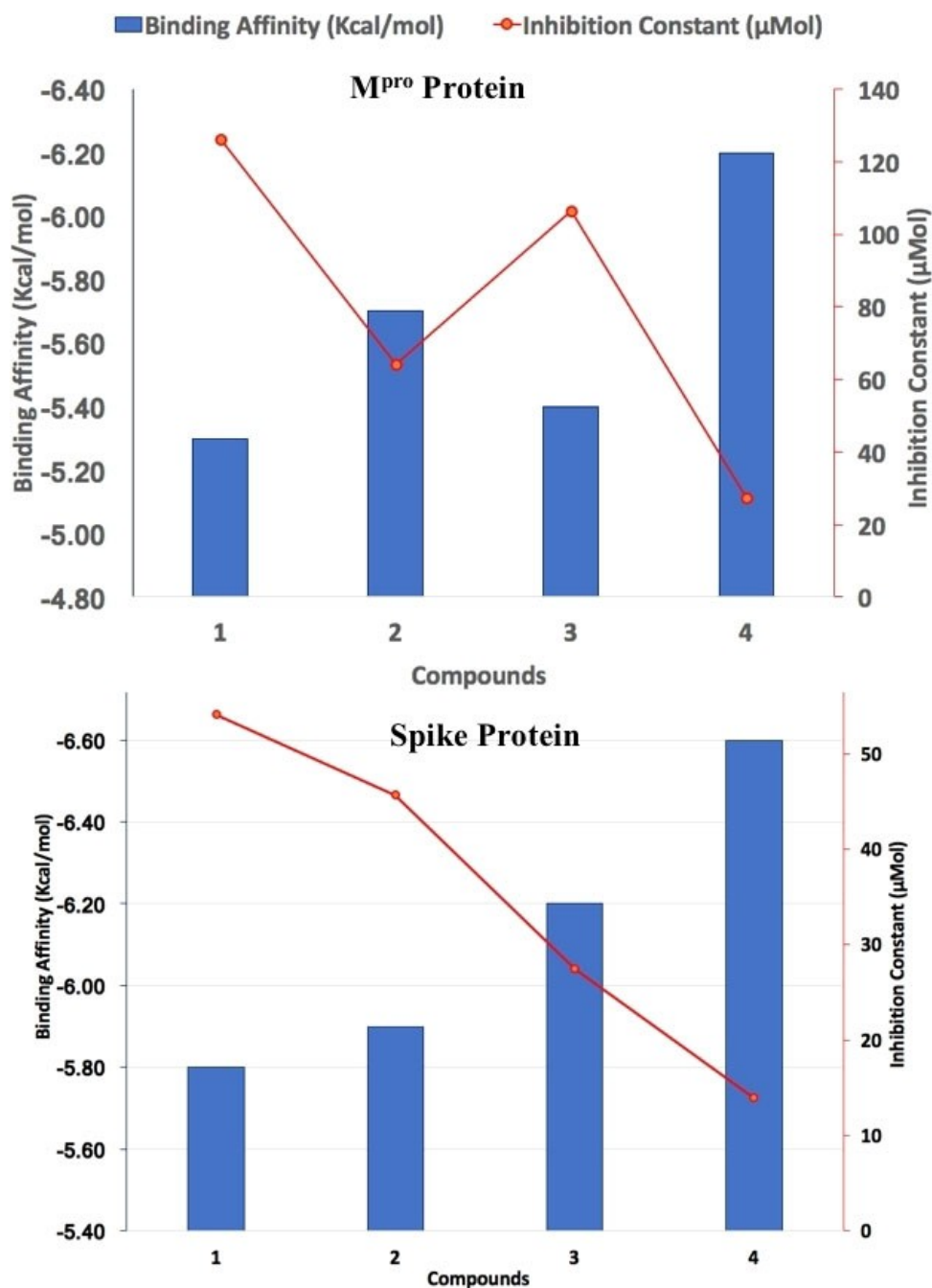


**Figure 6.** The graphical representation of binding interaction energies of compound 1–4 with M<sup>pro</sup> and spike protein of SARS-CoV-2.

compounds as synthesized and docked against Mpor enzyme showed binding energies ranging from  $-4.1$  (compound 1) to  $-8.5$  kcal/mol (compound 15).<sup>[39]</sup> The binding energy of our best docked complex in terms of E-score is also comparable to azo imidazole derivative (L3 =  $-6.7$  kcal/mol),<sup>[40]</sup> Chloroquine ( $-5.3$  kcal/mol), 6-Gingerol ( $-5.8$  kcal/mol) and Myristicin ( $-5.3$  kcal/mol) etc.<sup>[41]</sup> It is important to pen down that this semi-quantitative comparison based

only on binding energies as calculated through similar protocols using grid based docking techniques. The results should be carefully read considering many other drug-designing factors.

#### Visualization of Protein-Ligand Interactions

Though the binding energy and inhibition constants are important, it will also very useful to visualize the

intermolecular interactions among ligands and protein macromolecules. Based on the binding energy of compound **4**, it was selected to study the interaction of ligand-receptor protein complex. The data in the Table 3 shows that binding energy of compound **4** with the spike protein is better than that of M<sup>Pro</sup>. The M<sup>Pro</sup> protein chain is composed of 306 residues. The active site of protease is activated by a protonation reaction in the catalytic site. The interactions of compound **4** with M<sup>Pro</sup> showed the highest interactions with six residues of the M<sup>Pro</sup> including three H-bonds with ASN142, SER144, CYS145 and two hydrophobic interactions CYS145 and ASN124. While on the other hands, spike protein consists of 1281 amino acid residues and compound **4** reacts with six residues of the spike protein including four H-bonds which consists of SERL28, AGR408, SERL96 and SERL97. The protein-ligand interactions in 3D and 2D representations for compound **4** with M<sup>Pro</sup> and spike proteins are shown in Figure 7. Furthermore, we have also drawn

the total density surfaces of both M<sup>Pro</sup> and spike proteins while interacting with ligand as shown in Figure 8. The Figure 8 also gives an overview about the orientation of ligand and its H-bonding and ionizability characteristics with over the density surface of both studied proteins.

#### Pharmacokinetic Properties and Lipinski's Rule of 5

The well-known Lipinski's rule of 5 was used to predict the drug likeness through pkCSM server.<sup>[42]</sup> According to this rule, any ligand is considered as a drug-like if it meets certain requirements including molecular weight < 500 g/mol, number of H-bond acceptor < 10, number of H-bond donors < 5 and lipophilicity represented as log P < 5 (Lipinski 2004).<sup>[43]</sup> In fact, all these molecules under investigation are said to have good absorption, low toxicity level good oral bioavailable permeable properties. The isolated all compounds obey Lipinski's rule 5. The bioavailability radar enables

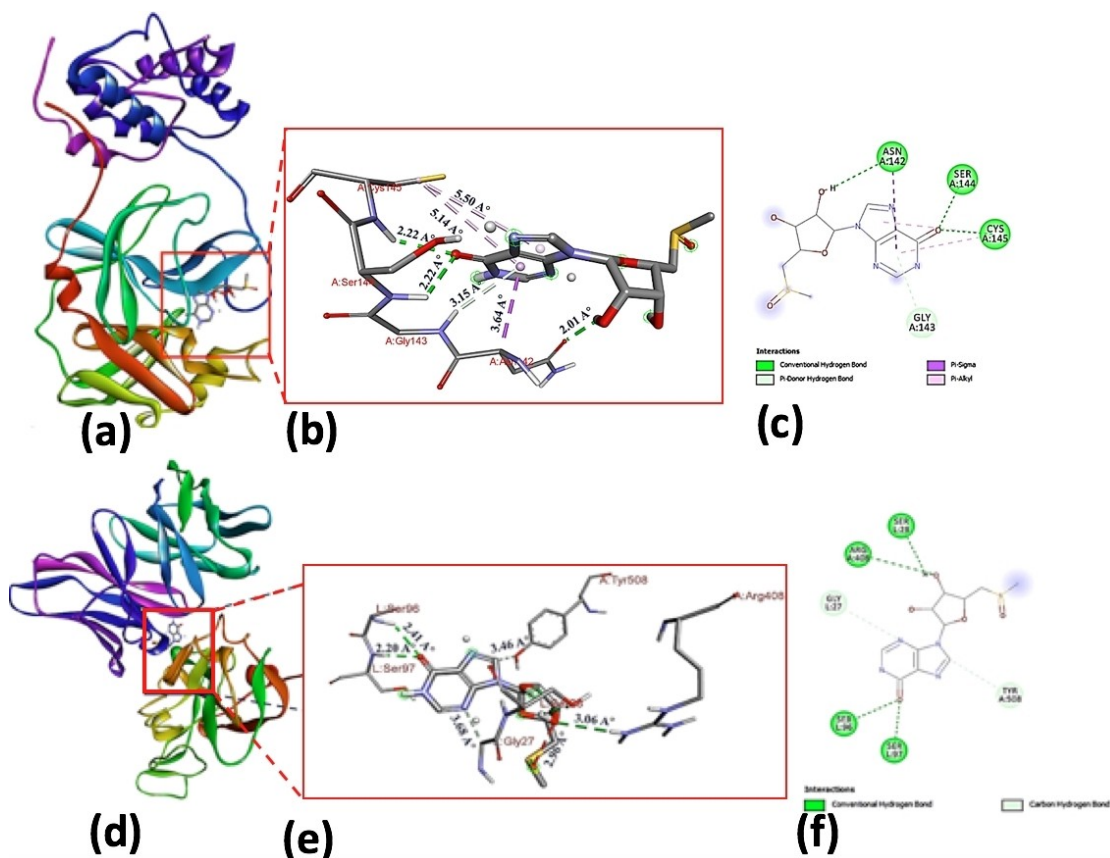


**Figure 7.** The protein-ligand interactions in 3D and 2D representations for compound **4** with M<sup>Pro</sup> and spike proteins: (a) whole M<sup>Pro</sup> protein showing docked compound **4** (b) focused view showing intermolecular bonding (c) 2D representation of compound **4** with interaction residues (d) whole spike protein showing docked compound **4** (e) focused view showing intermolecular bonding (f) 2D representation of compound **4** with interacting residues of spike protein.

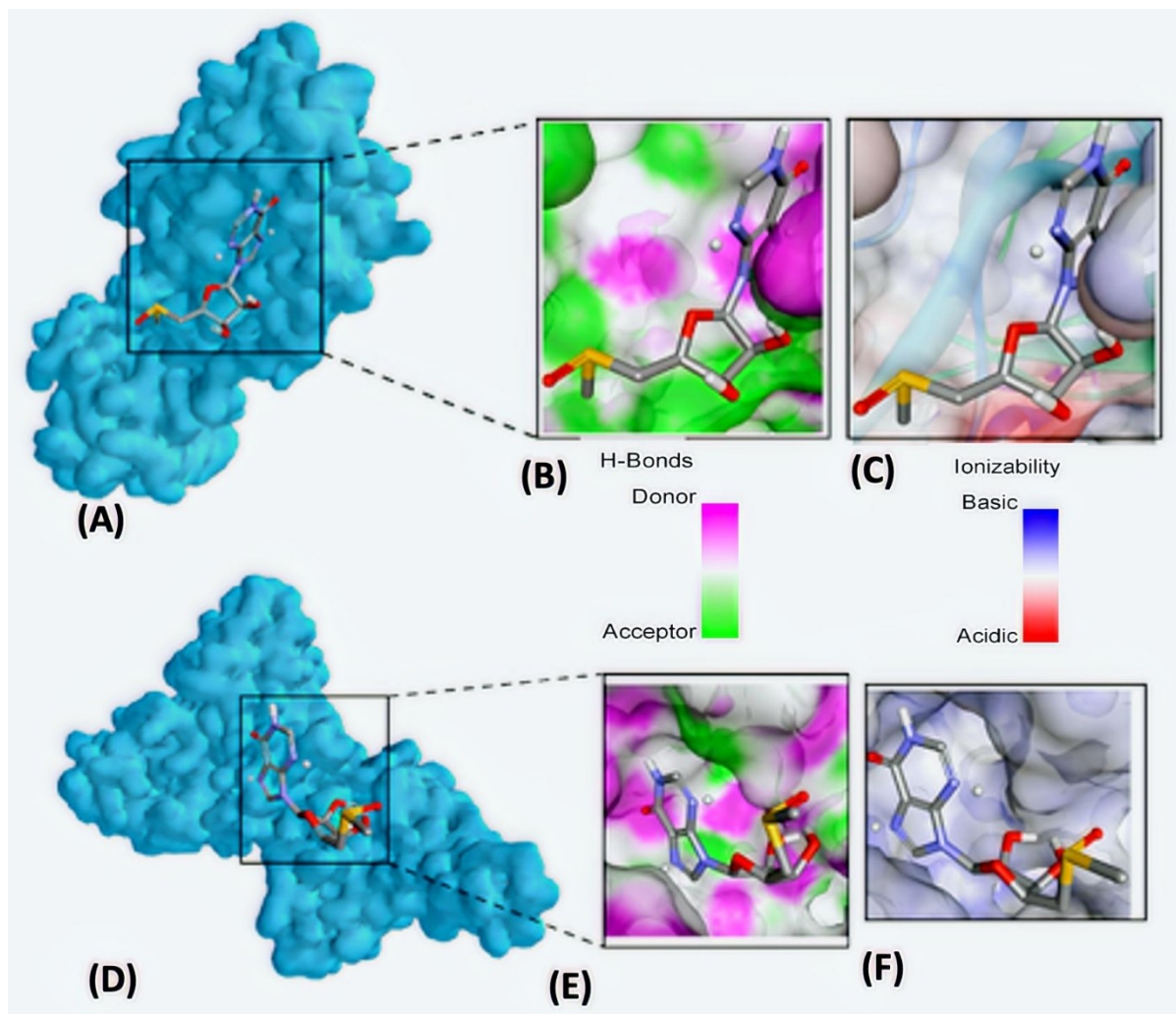


**Figure 8.** (A) Total surface density of docked compound **4** within cavity of  $M^{\text{pro}}$  protein, (B) hydrogen bond donor and acceptor meshes represented by pink and green colors, (C) representation inter-polated charges for basic and acidic pockets with blue and red colors, respectively, (D) total surface density of docked compound **4** within cavity of spike protein, (E) hydrogen bond donor and acceptor meshes represented by pink and green colors, (F) representation interpolated charges.

a first glance at the drug likeness of a molecule.<sup>[44]</sup> The pink area represents the optimal range for each propriety of drug likeness with normal range. The bioavailability radar (Figure 9) of the four selected molecules under investigation shown to further confirm their drug likeness properties where all the five crucial drug likeness parameters are in color area which is safe to use as drugs.

## Conclusion

The present study result in isolation of four new metabolites (**1–4**) from a terrestrial *Actinomycetes* sp. GSCW-51 which belong to thioinosine and butenolides

classes. The structure of the all the compounds were established through detail spectroscopic data. Furthermore, computational docking studies have shown a decent potential of our isolated compounds for inhibition of SARS-CoV-2 by interacting with its two very crucial  $M^{\text{pro}}$  and spike proteins. All the four compounds have shown the different values of favorable binding energies with  $M^{\text{pro}}$  and spike proteins. The binding energy of compounds **1–4** with  $M^{\text{pro}}$  protein are found to be  $-5.3$ ,  $-5.7$ ,  $-5.4$  and  $-6.2$  kcal/mol, respectively. The increasing order (where negative sign indicates favorable interactions) of binding energies is  $4 > 3 > 2 > 1$  for  $M^{\text{pro}}$  protein. While on the other hands, the binding energy of compounds **1–4** with spike protein are found to be

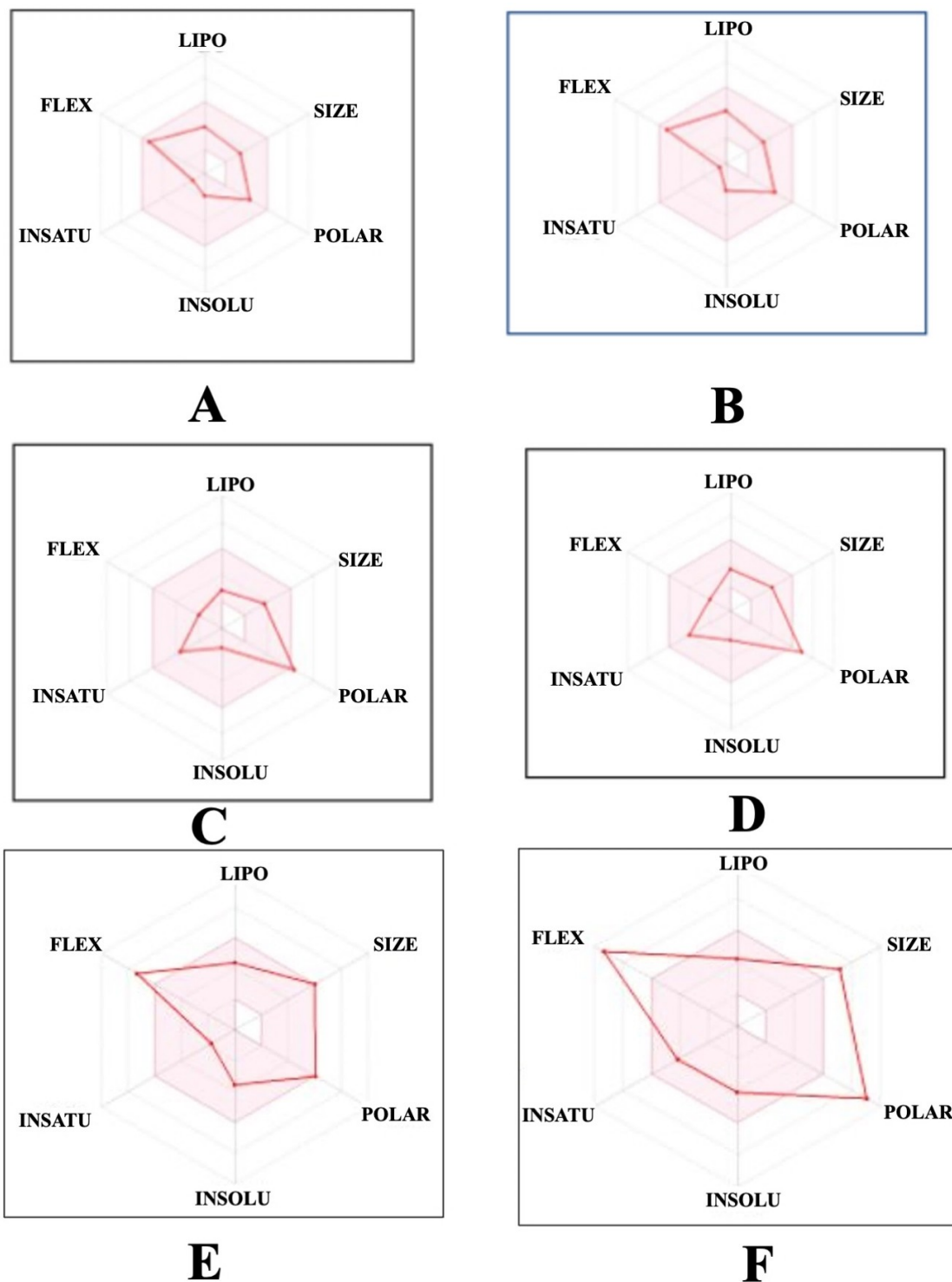


**Figure 9.** The bioavailability radar of all compounds: (A) compound 1, (B) compound 2, (C) compound 3, (D) compound 4, (E) Remdesivir and (F) Nirmatrelvir taken from SwissADME.

−5.8, −5.9, −6.2 and −6.6 kcal/mol, respectively. A careful analysis of results indicated that the compound 4 possessed the best binding energies of −6.2 and

−6.6 kcal/mol for M<sup>pro</sup> and spike proteins, respectively. Additionally, a renowned Lipinski's rule of 5 was used to predict the drug likeness of compounds 1–4, which

indicated all compounds obey Lipinski's rule 5. The study of bioavailability radar of the compounds **1–4** has shown and further confirm their drug likeness properties where all the five crucial drug likeness parameters are in color area which is safe to be used as drugs. Thus, our study encourages the *in vitro* or *in vivo* investigation to find the lead in our isolated compounds.

## Experimental Section

### General Experimental Procedures

Open column chromatography was performed on reversed phase silica gel RP-8 (10  $\mu$ m, Merck, Darmstadt Germany). IR spectra were measured on a PerkinElmer 1600 Series FT-IR spectrometer (KBr pellets). NMR spectra were recorded on Varian Inova 600 spectrometers. ESI HR mass spectra were recorded on A Bruker FTICR 4.7 T mass spectrometer. ESI mass spectra were recorded on a Finnigan MAT95 spectrometer at 70 eV. Optical rotations were measured on a Perkin Elmer polarimeter 241. Thin layer chromatography was performed on Polygram SIL G/UV254 (Macherey-Nagel & Co.). Size exclusion chromatography was done on Sephadex LH-20 (Pharmacia). Commercial solvents (dichloromethane, ethyl acetate, methanol) were used after distillation and malt extract (Merck-Germany) for media preparation.

### Isolation, Identification, Cultivation of Bacteria and Extraction

The sandy soil sample was collected from the top 5 cm of earth surface and packed in sterile plastic polythene bags. The collected sample was air dried for one week and further heat treatment was done in a hot air oven at 120 °C for 1 h in order to prevent growth of other bacteria.<sup>[45]</sup> Microscopic morphological, physiological study and biochemical analysis was carried out according to the reported method<sup>[46–48]</sup> to identify the isolated *Actinomyces* sp. GSCW-51.

A 15.0 L of culture media (200 g malt extract, 80.0 gm yeast extract and 80 gm glucose in tap water, pH 7.8) was prepared and transferred to 1.0 L Erlenmeyer flasks (250 ml each). The media was autoclaved at 120 °C for 15 min and was infected by the pre-cultured terrestrial *Actinomyces* sp. GSCW-51. The flasks were then incubated on a linear shaker (110 rpm) at 28 °C for 8 days until the broth attained dark brown color. The culture broth was harvested

after 8 days, filtered under vacuum and was extracted with AcOEt to get dark brown gummy mass. The bacterial mass was also extracted with methanol, and both the extract were mixed to get total crude extract (4.0 g).

### Isolation and Characterization of Compounds **1–4**

The crude extract was suspended in water (1.0 L) and was extracted with CH<sub>2</sub>Cl<sub>2</sub> to remove unwanted non-polar compounds/lipids. The remaining aqueous layer was extracted with ethyl acetate to yield a condensed organic material (1.5 g). The ethyl acetate extract was loaded on a silica gel column and eluted with a gradient mobile phase starting from CH<sub>2</sub>Cl<sub>2</sub> to a mixture of CH<sub>2</sub>Cl<sub>2</sub>/MeOH (85:150) to get 4 main fractions based on TLC profiles. Fraction 2 showed a complex TLC profile and thus was subjected to gel filtration using Sephadex LH-20 eluting with MeOH resulting in another sub-fraction. This fraction was then repeatedly chromatographed over an RP-8 open column using 40% aqueous methanol to get tyrosol (**8**, 5.8 mg), 4-(4'-hydroxyphenyl)butan-2-one (**7**, 5.1 mg), 3-methoxy-4-hydroxybenzoic acid (**6**, ~3.0 mg), 3-methoxy-4,5-dihydroxybenzoic acid (**5**, 4.0 mg) and another impure fraction, which was further separated on RP-8 silica column using 35% aqueous methanol as eluting solvent to get compound **1** (~2.7 mg) and compound **2** (~3.5 mg). Fraction 3 from main column was also cleaned over Sephadex LH-20 eluting with methanol and the resulting material was chromatographed on silica gel using CH<sub>2</sub>Cl<sub>2</sub>/MeOH (90:10) as mobile phase that yielded two sub-fractions (3a and 3b). Fraction 3a was then subjected to RP-8 open column eluting with 25% aqueous methanol to yield compound **3** and **4** (~5.0 mg each).

**5-Hydroxymethyl-3-(1-hydroxy-6-methyl-7-oxo-octyl)dihydrofuran-2(3H)-one (1)**: (for the spectral data, please see the *Supporting Information*).

**5-Hydroxymethyl-3-(1,7-dihydroxy-6-methyl-octyl)dihydrofuran-2(3H)-one (2)**: (for the spectral data, please see the *Supporting Information*).

**5'-Methylthioinosine (3)**: (for the spectral data, please see the *Supporting Information*).

**5'-Methylthioinosine sulfoxide (4)**: (for the spectral data, please see the *Supporting Information*).

## Computational Methodology

All molecular docking calculations were performed through Autodock Vina (ADV).<sup>[49]</sup> Besides this MGL tools<sup>[50]</sup> and Discovery Studio Visualizer<sup>[51]</sup> are used for intermolecular interaction analysis. The SARS-CoV-2 proteins including main protease (MPro) (6lu7)<sup>[52]</sup> and spike (7jva)<sup>[53]</sup> proteins were retrieved from protein data bank<sup>[54]</sup> in pdb formats. The PDB files of both compounds and proteins were converted into an extended PDB format which is termed as PDBQT for performing molecular docking analysis. The grid parameters were written into a configuration file. The docked conformations with the lowest binding energy were considered as the most stable conformations of the compounds within the respect macromolecules. As ADV based is on grid methods so the most important step in molecular docking is assigning the grid parameters since it navigates the ligand to the binding site of the protease. The center grid box values for M<sup>Pro</sup> were set to center x = 25, center y = 12 center z = 57 and grid box dimensions (angstrom) were set to x = 73, y = 81, z = 78. The center grid box values for spike protein were set to center x = 204, y = 205, z = 202 and number of grid box dimension (angstrom) were set to x = 195, y = 138, z = 138. These parameters were set to cover the entire 3-dimensional active sites of the protease and spike proteins. The outputs were saved in the grid parameter file formats, which were later used for visualization process.

## Acknowledgements

M.N and M. I. T thanks the German Academic Exchange Program (DAAD), Germany and HEC Pakistan SRGP grant No. 1543, for their support. The authors also extend their appreciation to Deanship of Scientific Research at King Khalid University for funding the work through Research Project (RGP.2/156/42). For computer time, this research used the resources of the Supercomputing Laboratory at King Abdullah University of Science & Technology (KAUST) in Thuwal, Saudi Arabia.

## Conflict of Interest

The authors declare no conflict of interest.

## Author Contribution Statement

M. N., S. P., N. A., N. F. and M. I. T. Conceptualization, Methodology, performed the experiments and Isolation of compounds. R. F. M. and M. F. M. data analysis, Writing original draft. M. K., M. U. K., S. M. and S. S. A. Conceptualization, writing original draft, Software, Docking studies.

## References

- [1] K. Jakubiec-Krzesniak, A. Rajnisz-Mateusiak, A. Guspiel, J. Ziemska, J. Solecka, 'Secondary metabolites of actinomycetes and their antibacterial, antifungal and antiviral properties', *Pol. J. Microbiol.* **2018**, *67*, 259.
- [2] E. A. Barka, P. Vatsa, L. Sanchez, N. Gaveau-Vaillant, C. Jacquard, H.-P. Klenk, C. Clément, Y. Ouhdouch, G. P. van Wezel, 'Taxonomy, physiology, and natural products of Actinobacteria', *Microbiol. Mol. Biol. Rev.* **2016**, *80*, 1–43.
- [3] K. F. Chater, 'Recent advances in understanding Streptomyces', *F1000Research* **2016**, *5*.
- [4] X. Guo, N. Liu, X. Li, Y. Ding, F. Shang, Y. Gao, J. Ruan, Y. Huang, 'Red soils harbor diverse culturable actinomycetes that are promising sources of novel secondary metabolites', *Appl. Environ. Microbiol.* **2015**, *81*, 3086–3103.
- [5] S. M. Pimentel-Elardo, S. Kozzytska, T. S. Bugni, C. M. Ireland, H. Moll, U. Hentschel, 'Anti-parasitic compounds from Streptomyces sp. strains isolated from Mediterranean sponges', *Mar. Drugs* **2010**, *8*, 373–380.
- [6] S. A. Waksman, A. Schatz, D. M. Reynolds, 'Production of antibiotic substances by actinomycetes', *Ann. N. Y. Acad. Sci.* **2010**, *1213*, 112–124.
- [7] A. Raveh, P. C. Delekta, C. J. Dobry, W. Peng, P. J. Schultz, P. K. Blakely, A. W. Tai, T. Matainaho, D. N. Irani, D. H. Sherman, D. J. Miller, 'Discovery of potent broad spectrum antivirals derived from marine actinobacteria', *PLoS One* **2013**, *8*, e82318.
- [8] Y. Kato, 'Ethyl 3, 4-dihydroxy-5-methoxybenzoate, an intermediate product for the synthesis of 3, 4-dihydroxy-5-methoxybenzoic acid', *Org. Prep. Proced. Int.* **1981**, *13*, 172–175.
- [9] F. L. P. Costa, F. das Neves, A. C. F. de Albuquerque, F. M. dos Santos Junior, G. G. Leitão, M. B. de Amorim, 'Bathysa australis Vanillic Acid (4-hydroxy-3-methoxybenzoic acid) Isolation by Countercurrent Chromatographic and Characterization by NMR 1H and 13C Experimental and Theoretical GIAO-B3PW91/cc-pVDZ//B3PW91/cc-pVDZ Chemical Shifts', *J. Comput. Theor. Nanosci.* **2014**, *11*, 1732–1737.
- [10] D. Chung, S. Y. Kim, J.-H. Ahn, 'Production of three phenylethanoids, tyrosol, hydroxytyrosol, and salidroside, using plant genes expressing in Escherichia coli', *Sci. Rep.* **2017**, *7*, 1–8.
- [11] J. Beekwilder, I. M. van der Meer, O. Sibbesen, M. Broekgaarden, I. Qvist, J. D. Mikkelsen, R. D. Hall, 'Microbial production of natural raspberry ketone', *Biotechnol. J.* **2007**, *2*, 1270–1279.

- [12] H. Laatsch, 'A data base for rapid structural determination of microbial natural products, and annual updates', <http://www.user.gwdg.de/~ucoc/laatsch/AntiBase.htm>, **2010**.
- [13] T. Řezanka, M. Temina, L. Hanuš, V. M. Dembitsky, 'The tornabeatins, four tetrahydro-2-furanone derivatives from the lichenized ascomycete *Tornabea scutellifera* (With.) JR Laundon', *Phytochemistry* **2004**, *65*, 2605–2612.
- [14] C. Pathirana, R. Dwight, P. R. Jensen, W. Fenical, A. Delgado, L. S. Brinen, J. Clardy, 'Structure and synthesis of a new butanolide from a marine actinomycete', *Tetrahedron Lett.* **1991**, *32*, 7001–7004.
- [15] R. P. Maskey, Neuartige Wirkstoffe aus marinen Streptomyceten: Sagunamycine, Parimycin, Himalomycine, Gottingamycin, Dhanyabadomycin, Akashine und stark cytotoxische Trioxacarcine mit hoher Antimalarial-Aktivität, **2001**.
- [16] W. Aruna, J. W. Anura, C. Gavin, W. David, A. Raymond, K. Veranja, 'Gardinerin, a biologically active acetogenin from the sri lankan goniothalamus *gardineri* hook. F. and thomson', *Int. J. Pharm. Pharm. Sci.* **2015**, *7*, 459–461.
- [17] C.-Y. Chen, 'Butanolides from the stem of *Cinnamomum kotoense*', *Nat. Prod. Commun.* **2006**, *1*, 1934578X0600100604.
- [18] B. M. Fraga, D. Terrero, 'Alkene- $\gamma$ -lactones and avocadofurans from *Persea indica*: A revision of the structure of majorenolide and related lactones', *Phytochemistry* **1996**, *41*, 229–232.
- [19] M.-L. Wang, J. Du, P.-C. Zhang, R.-Y. Chen, F.-Z. Xie, B. Zhao, D.-Q. Yu, 'Saccopetrins A and B, two novel  $\gamma$ -lactones from *Saccopetalum prolificum*', *Planta Med.* **2002**, *68*, 719–722.
- [20] V. J. Mukku, M. Speitling, H. Laatsch, E. Helmke, 'New butanolides from two marine streptomycetes', *J. Nat. Prod.* **2000**, *63*, 1570–1572.
- [21] M. A. Ouyang, 'A new adenosyl-alkaloid from *Ostrea rivularis*', *Nat. Prod. Res.* **2006**, *20*, 79–83.
- [22] Y. Doi, M. Ishibashi, J. I. Kobayashi, 'Isolation and structure of shimofuridins B~G from the Okinawan marine tunicate *Aplidium multiplicatum*', *Tetrahedron* **1994**, *50*, 8651–8656.
- [23] P. Ciuffreda, A. Loseto, L. Alessandrini, G. Terraneo, E. Santaniello, 'Adenylate Deaminase (5'-Adenylic Acid Deaminase, AMPDA)-Catalyzed Deamination of 5'-Deoxy-5'-Substituted and 5'-Protected Adenosines: A Comparison with the Catalytic Activity of Adenosine Deaminase (ADA)', *Eur. J. Org. Chem.* **2003**, *2003*, 4748–4751.
- [24] C. J. Cramer, 'Hyperconjugation as it affects conformational analysis', *J. Mol. Struct.* **1996**, *370*, 135–146.
- [25] H. Kawagishi, F. Fukuhara, M. Sazuka, A. Kawashima, T. Mitsubori, T. Tomita, '5'-Deoxy-5'-methylsulphinyladenosine, a platelet aggregation inhibitor from *Ganoderma lucidum*', *Phytochemistry* **1993**, *32*, 239–241.
- [26] M. Marrelli, V. Amodeo, G. Statti, F. Conforti, 'Biological properties and bioactive components of *Allium cepa* L.: Focus on potential benefits in the treatment of obesity and related comorbidities', *Molecules* **2019**, *24*, 119.
- [27] S. Salama, T. Dishisha, M. H. Habib, A. Z. Abdelazem, W. Bakeer, M. Abdel-Latif, Y. Gaber, 'Enantioselective sulfoxidation using *Streptomyces glaucescens* GLA. 0', *RSC Adv.* **2020**, *10*, 32335–32344.
- [28] Y. Sun, J. Liu, L. Li, C. Gong, S. Wang, F. Yang, H. Hua, H. Lin, 'New butanolide derivatives from the marine sponge-derived fungus *Aspergillus terreus*', *Bioorg. Med. Chem. Lett.* **2018**, *28*, 315–318.
- [29] W. Gu, C. Qiao, 'Furandiones from an endophytic *Aspergillus terreus* residing in *Malus halliana*', *Chem. Pharm. Bull.* **2012**, *60*, 1474–1477.
- [30] F. Guo, Z. Li, X. Xu, K. Wang, M. Shao, F. Zhao, H. Wang, H. Hua, Y. Pei, J. Bai, 'Butanolide derivatives from the plant endophytic fungus *Aspergillus terreus*', *Fitoterapia* **2016**, *113*, 44–50.
- [31] Z. Wang, X. Hu, Y. Li, X. Mou, C. Wang, X. Chen, Y. Tan, C. Wu, H. Liu, H. Xu, 'Discovery and SAR Research for Antivirus Activity of Novel Butanolide on Influenza A Virus H1N1 *in vitro* and *in vivo*', *ACS Omega* **2019**, *4*, 13265–13269.
- [32] C.-Y. Chung, C.-H. Liu, G.-H. Wang, A. Jassey, C.-L. Li, L. Chen, M.-H. Yen, C.-C. Lin, L.-T. Lin, '(4R,6S)-2-dihydropyridin-6-ylidene is a butanolide that efficiently inhibits hepatitis C virus entry', *Sci. Rep.* **2016**, *6*, 1–11.
- [33] M. A. Abu-Zaied, S. F. Hammad, F. T. Halaweish, G. H. Elgemeie, 'Sofosbuvir Thio-Analogues: Synthesis and Antiviral Evaluation of the First Novel Pyridine-and Pyrimidine-Based Thioglycoside Phosphoramidates', *ACS Omega* **2020**, *5*, 14645–14655.
- [34] K. Yamamoto, M. Hasobe, M. Saneyoshi, 'Inhibitory effect of sulphur-containing purine nucleoside analogues on replication of RNA viruses: selective antiviral activity against influenza viruses', *Acta Virol. (Engl. Ed.)* **1988**, *32*, 386–392.
- [35] N. A. Van Draanen, G. A. Freeman, S. A. Short, R. Harvey, R. Jansen, G. Szczech, G. W. Koszalka, 'Synthesis and antiviral activity of 2'-deoxy-4'-thio purine nucleosides', *J. Med. Chem.* **1996**, *39*, 538–542.
- [36] S. Muhammad, S. H. Hassan, A. G. Al-Sehemi, H. A. Shakir, M. Khan, M. Irfan, J. Iqbal, 'Exploring the new potential antiviral constituents of *Moringa oleifera* for SARS-CoV-2 pathogenesis: An *in silico* molecular docking and dynamic studies', *Chem. Phys. Lett.* **2021**, *767*, 138379.
- [37] J. Gao, F. Sun, 'Drug discovery to treat COVID-19 two years after its outbreak', *Drug Discov. Ther.* **2021**, *15*, 281–288.
- [38] D. V. Parums, 'Current Status of Oral Antiviral Drug Treatments for SARS-CoV-2 Infection in Non-Hospitalized Patients', *Med. Sci. Monit.* **2022**, *28*, e935952.
- [39] E. Abdel-Latif, T. Khatib, A. Fekri, M. Khalifa, 'Synthesis of New Binary Thiazole-Based Heterocycles and Their Molecular Docking Study as COVID-19 Main Protease (Mpro) Inhibitors', *Russ. J. Gen. Chem.* **2021**, *91*, 1767–1773.
- [40] A. Chhetri, S. Chhetri, P. Rai, D. K. Mishra, B. Sinha, D. Brahman, 'Synthesis, characterization and computational study on potential inhibitory action of novel azo imidazole derivatives against COVID-19 main protease (Mpro: 6LU7)', *J. Mol. Struct.* **2021**, *1225*, 129230.
- [41] T. E. Tallei, S. G. Tumilaar, N. J. Niode, B. J. Kepel, R. Idroes, Y. Effendi, S. A. Sakib, T. B. Emran, 'Potential of plant bioactive compounds as SARS-CoV-2 main protease (Mpro) and spike (S) glycoprotein inhibitors: a molecular docking study', *Scientifica* **2020**, *2020*.
- [42] D. E. Pires, T. L. Blundell, D. B. Ascher, 'pkCSM: predicting small-molecule pharmacokinetic and toxicity properties using graph-based signatures', *J. Med. Chem.* **2015**, *58*, 4066–4072.

- [43] C. A. Lipinski, 'Lead- and drug-like compounds: the rule-of-five revolution', *Drug Discovery Today Technol.* **2004**, *1*, 337–341.
- [44] A. Daina, O. Michielin, V. Zoete, 'SwissADME: a free web tool to evaluate pharmacokinetics, drug-likeness and medicinal chemistry friendliness of small molecules', *Sci. Rep.* **2017**, *7*, 42717.
- [45] A. A. Aliero, I. Ntulume, J. Odda, M. A. Okech, 'Production of novel antifungal compounds from actinomycetes isolated from waste dump soil in Western Uganda', *Afr. J. Microbiol. Res.* **2017**, *11*, 1200–1210.
- [46] G. E. Daigham, A. Y. Mahfouz, 'Isolation, characterization, and screening of actinomycetes producing bioactive compounds from Egyptian soil', *Egypt. Pharm. J.* **2020**, *19*, 381.
- [47] W. P. Njenga, F. B. Mwaura, J. M. Wagacha, E. M. Gathuru, 'Methods of Isolating Actinomycetes from the Soils of Menengai Crater in Kenya', *Arch. Clin. Microbiol.* **2017**, *8*, 45.
- [48] V. Dhananjeyan, N. Selvan, K. Dhanapal, 'Isolation, characterization, screening and antibiotic sensitivity of Actinomycetes from locally (near MCAS) collected soil samples', *J. Biol. Sci.* **2010**, *10*, 514–519.
- [49] S. Dallakyan, A. J. Olson, in *Chemical biology*, Springer, **2015**, pp. 243–250.
- [50] E. Di Muzio, D. Toti, F. Polticelli, 'DockingApp: a user friendly interface for facilitated docking simulations with AutoDock Vina', *J. Comput.-Aided Mol. Des.* **2017**, *31*, 213–218.
- [51] D. Studio, 'Discovery Studio', Accelrys [2.1], **2008**.
- [52] S. Khaerunnisa, H. Kurniawan, R. Awaluddin, S. Suhartati, S. Soetjijpto, Potential inhibitor of COVID-19 main protease (Mpro) from several medicinal plant compounds by molecular docking study, **2020**.
- [53] J. Chen, K. Gao, R. Wang, G. W. Wei, 'Prediction and mitigation of mutation threats to COVID-19 vaccines and antibody therapies', *Chem. Sci.* **2021**, *12*, 6929–6948.
- [54] H. M. Berman, J. Westbrook, Z. Feng, G. Gilliland, T. N. Bhat, H. Weissig, I. N. Shindyalov, P. E. Bourne, 'The protein data bank', *Nucleic Acids Res.* **2000**, *28*, 235–242.

Received November 14, 2021

Accepted February 25, 2022